



I1.2.3 Deliverable – Geophysical imaging post-sampling report

Date: January, 2020



SUBJECT: ...

report
 information
 consideration
 decision

To: ... **From:** ULiege & BGS

Introduction

The following report describes the results of the post-sampling geophysical survey carried out in the former landfill of Meerhout, one of the pilot sites of the RAWFILL project. The purpose of the survey is to refine the geophysical images obtained during the first geophysical survey (see Deliverable I1.2.2) and improve correlations with the sampling results (see Deliverable I1.3.4).

The described investigations were conducted in January 30th - 31st 2019 and in April 2nd 2019. They were prepared in close coordination with OVAM and the members of the IOK (owner of the site). They follow the borehole sampling phase which was carried out in November 2018 and precede the digging of the trench (which was carried out on April 8th 2019).

Summary of the study area and previous investigations

The Meerhout landfill contains mainly household and industrial wastes that were deposited between 1962 until 1997. More information about the site can be found in Deliverable I1.1.1. During the first geophysical survey (see Deliverable I1.2.2), two zones of the landfill were particularly investigated (see Fig. 1). Based on the results obtained, a sampling plan was proposed and consisted in 11 boreholes and 1 trench of 50 m long (cf. Deliverable I1.3.1). Due to the presence of buried gas extraction pipes, only 9 of the foreseen boreholes could be drilled and the proposed trench had to be shifted northwards. Their final location is shown in Fig. 1.

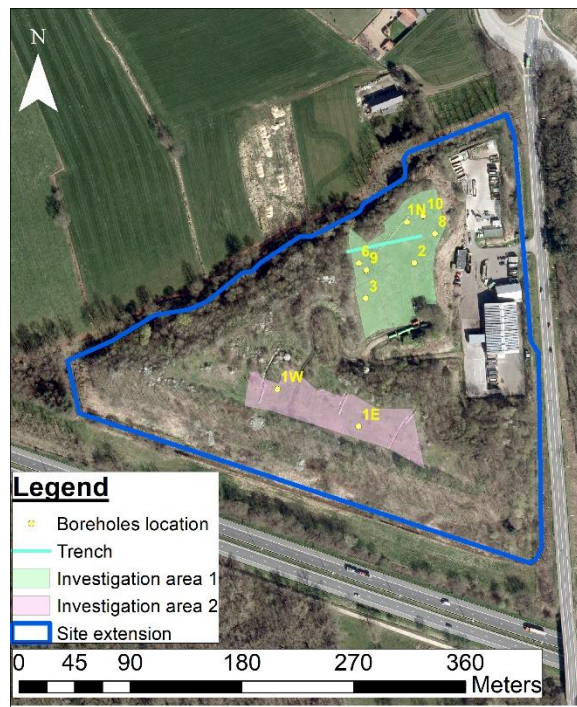


Figure 1: Areas investigated during the first geophysical survey and sampling locations

Sampling data provided valuable information regarding the landfill geometry and composition. In investigation area 1, the thickness of the landfill was measured between 11.5 (borehole 10) to 14 m (borehole 6) including a 1 to 2 m cover layer. The latter is mainly composed of inerts (moderately coarse sand with brick pieces, little gravels and some debris). The body waste found below the cover layer is mainly composed of household waste with plastics, textiles, metals, leather, rubber, gypsum waste and glass. A water table was detected at 7.5 m depth. In investigation area 2, the thickness of the landfill is much larger (around 24 m) with a 1 to 2 m cover layer. The types of waste found in area 2 are similar to those observed in area 1. Below the waste body, the natural soil is made of moderately coarse sand with moderate clay content from the Diest formation.

Geophysical investigations

In the following, all applied geophysical methods are listed with their expected main sensitivities on landfills. For a more detailed description of each geophysical method, please refer to the following report T1.3.1: Swot analysis of LF characterization methods.

In order to get a full areal coverage, the following mapping methods were used:

- **Electromagnetic (EM):** to reveal lateral extent of different waste composition or leachate content at several distinctive depths (mapping changes in electrical conductivity and magnetic susceptibility)

More focused 2D/3D surveys, providing detailed information about changes of physical properties with depth were done along distinct profiles including the following methods:

- **Ground Penetrating Radar (GPR):** to measure the thickness of the cover layers (registering the returned GPR signal which was reflected or diffracted at material boundaries with significant changes in relative electric permittivity).
- **Electrical Resistivity Tomography (ERT) and Induced Polarization (IP):** to discriminate different waste types, investigate changes in leachate content (measuring resistivity distribution) and to detect metallic scraps or zones of higher organic content (measuring chargeability distribution).



Figure 2: 3D electrical setup deployed in January 2019

Measurement systems and parameters

In the next section, the measurement parameters for each method are summarized.

The **electromagnetic** data was acquired using a conductivity meter model DUALEM-4. By attaching two different antennas sizes, mapping at four different depth levels could be achieved. These depths were 0.5 m and 2.3 m for the shorter antenna and 1.8 m and 5.3 m for the longer antenna. Both quadrature (related to apparent conductivity) and in-phase (related to apparent magnetic susceptibility) components were recorded simultaneously for each antenna. In addition, a GPS sensor (no RTK) was connected to the system for positioning. Separate acquisitions were performed along a grid with different interline spacings. A first acquisition was conducted on the whole investigation area 1 with the short antenna with an interline spacing of 3 m (see red dots in Fig. 3a). Then, using the same antenna, we focused on a smaller zone where the 3D ERT grid was setup using an interline spacing of 1.5 m (see blue dots in Fig. 3a). On the same smaller area, measurements were also collected with the longer antenna with an interline spacing of 3 m (see Fig.3b).

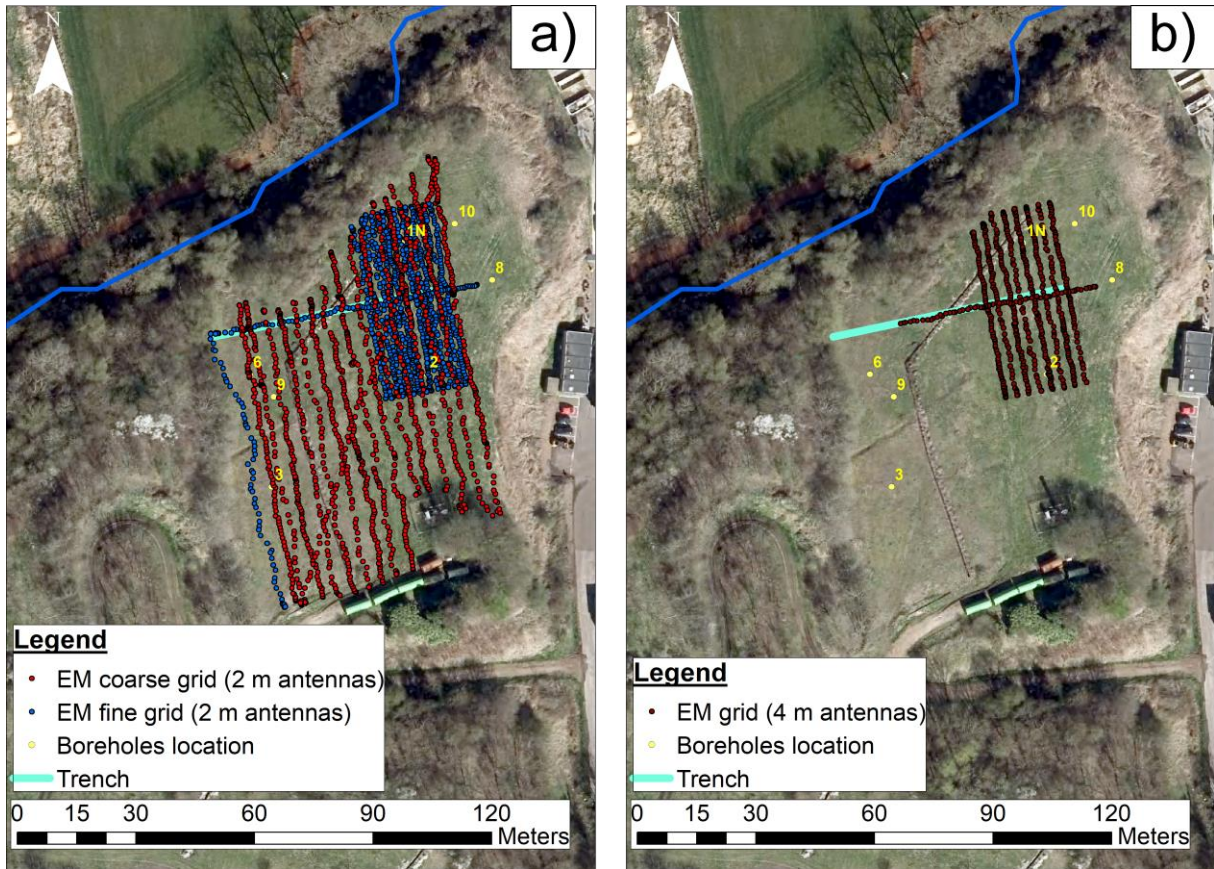


Figure 3: EM data coverage

The **ground penetrating radar (GPR)** was used to estimate the cover layer thickness. Several profiles were measured with a 250MHz antenna, which represents the best compromise between depth of investigation and resolution (to estimate the cover layer thickness). The antennas were mounted to a cart. The positioning was done with a odometer wheel. Measurements were carried out on the whole investigation area 1 along a grid with an interline spacing of 2 m (see Fig. 4).

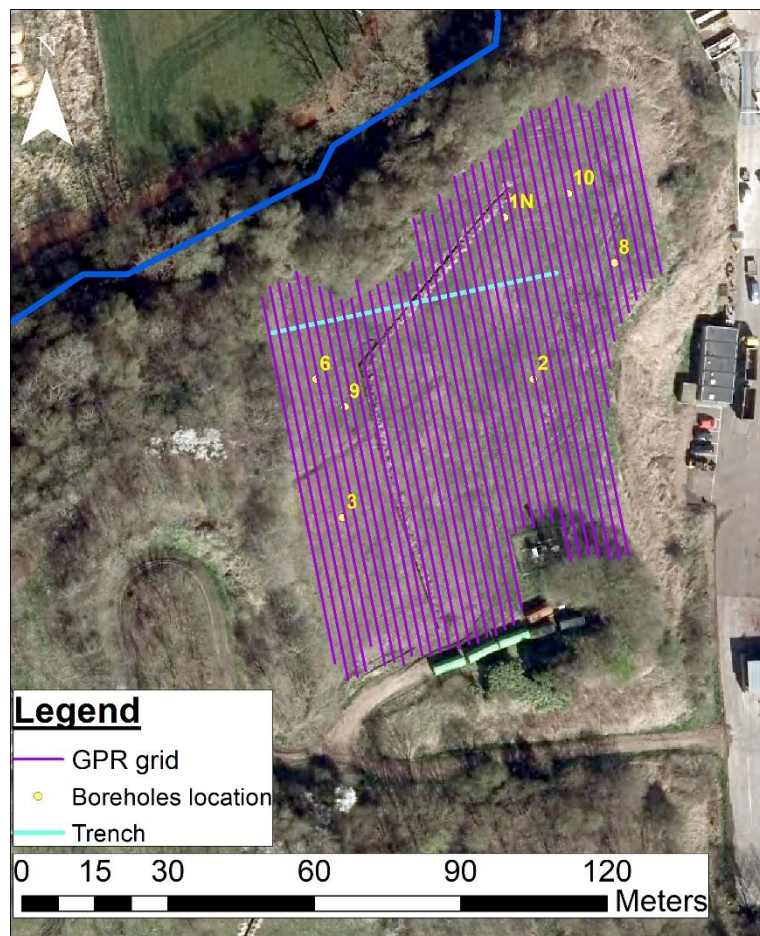


Figure 4: GPR grid

Electrical resistivity tomography (ERT) and time-domain induced polarization (TDIP or IP) data were acquired with an ABEM Terrameter LS system. Two separate electrical surveys were conducted. The first one carried out in January 2019 involved a 3D ERT data acquisition using the grid displayed in Fig. 5 (see red dots). For the data acquisition, we used a custom dipole-dipole configuration following the approach proposed in Van Hoorde et al. (2017). We deployed 8 lines of 32 stainless steel electrodes with an interline spacing of 3 m and an electrode spacing of 1.5 m. Measurements were repeated twice with an acquisition delay of 0.2 s and an acquisition time of 0.3 s. A sample of reciprocal data was also collected in order to build a data error model. The second survey was carried out in April 2019 just before the trench was dug. It consisted in a high resolution 2D ERT and IP profile using 110 stainless steel electrodes spaced by 0.75 m (see blue dots in Fig. 5). Electrical current injection was setup to 2 s (delay of 0.8 s and acquisition of 1.2 s) and voltage decay was measured for 2 s after current shut down. The protocol used is a dipole-dipole with the factor 'n' limited to 6 (Dahlin & Zhou 2004). By lack of time, no repetition nor reciprocal measurements could be collected.

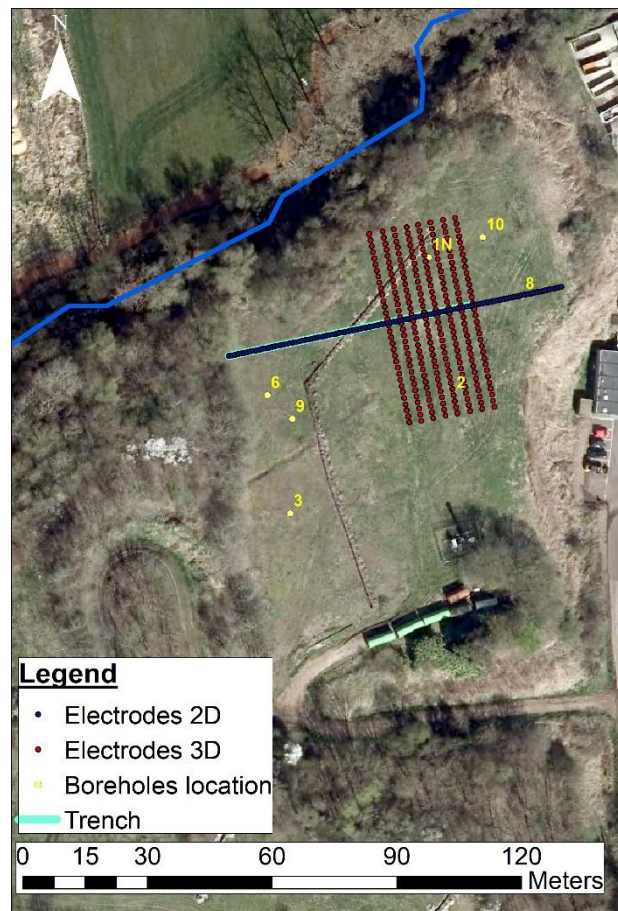


Figure 5: Electrodes used for the 3D ERT measurements (red dots) and 2D ERT and IP (blue dots). The latter is aligned with the trench.

Geophysical processing and results

EM

Figs. 6 to 9 displays the electrical conductivities measured with the electromagnetic system. Each figure compares the post sampling data, measured in January 2019 (B and C) with the pre-sampling data, measured in January 2018 (A). The electrical conductivity can, in addition to waste composition or cover layer thickness, be influence by moisture content. Hence, high conductivity variations between the pre- and the post sampling results might indicate a change in moisture content caused by the different weather conditions during and prior to the two surveys. However, at all four measured depths, the conductivity pattern seems to be consistent. This indicates similar moisture conditions during both surveys.

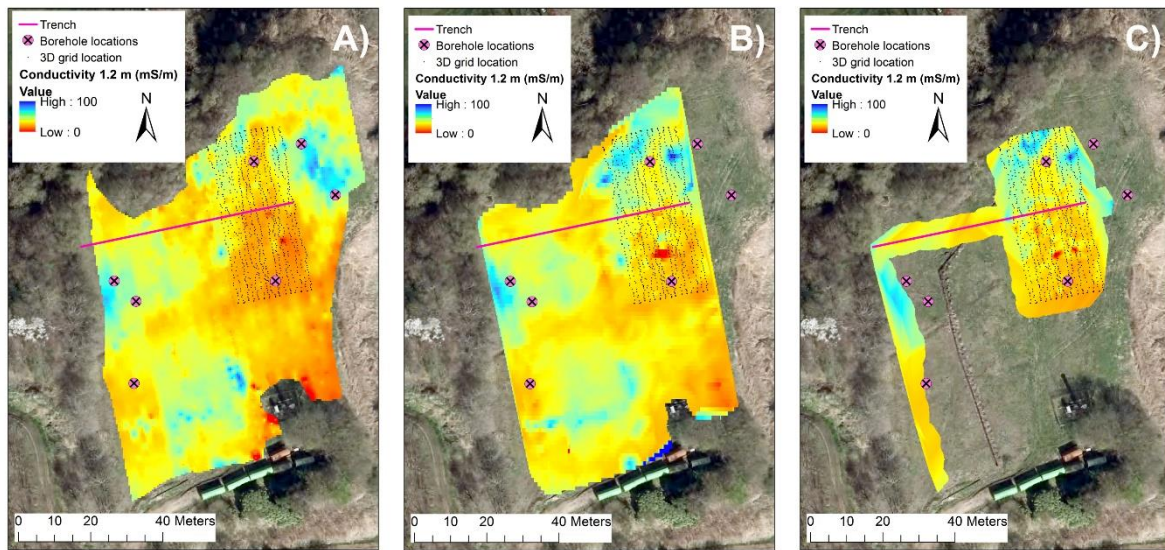


Figure 6: Electrical conductivity map at an investigation depth of 1.2 m below ground. This map was derived from the quadrature-phase data measured with the 2 m antenna and vertical coil alignment. A) Data measured during the pre-sampling survey in January 2018. B & C) Data measured during the post-sampling survey in January 2019 with C being the high resolution grid measured along the 3D ERT profiles.

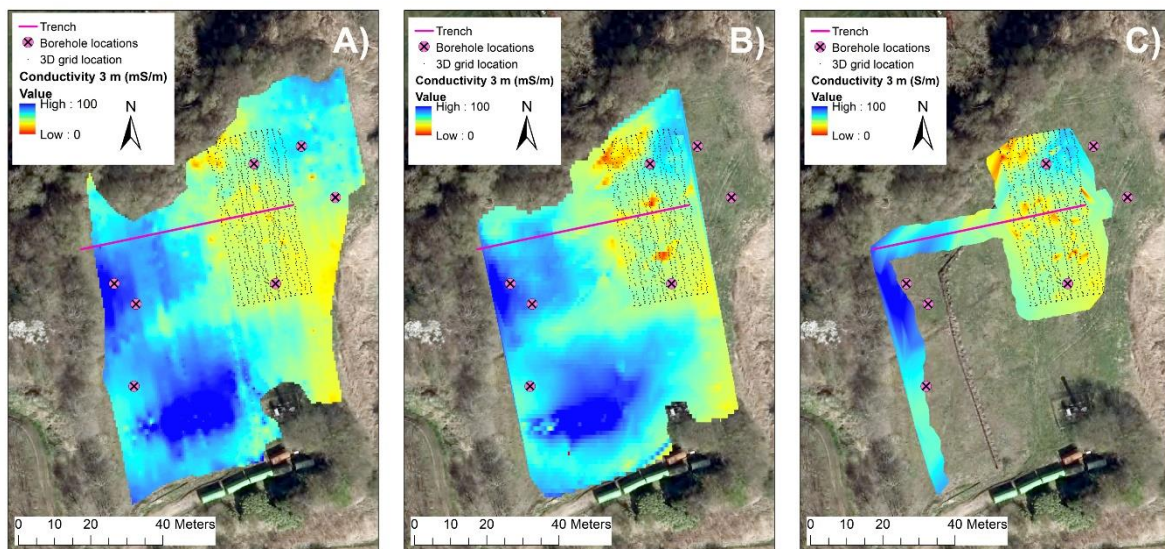


Figure 7: Electrical conductivity map at an investigation depth of 3 m below ground. This map was derived from the quadrature-phase data measured with the 2 m antenna and horizontal coil alignment. A) Data measured during the pre-sampling survey in January 2018. B & C) Data measured during the post-sampling survey in January 2019 with C being the high resolution grid along the 3D ERT profiles.

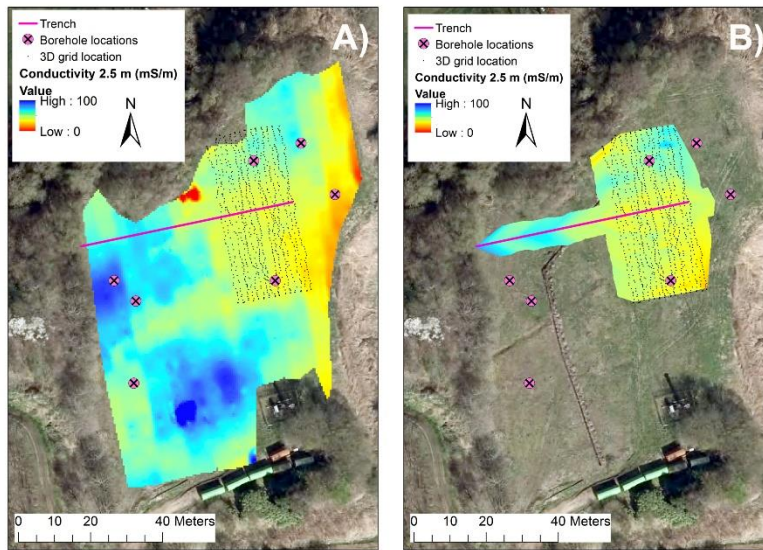


Figure 6: Electrical conductivity map at an investigation depth of 2.5 m below ground. This map was derived from the quadrature-phase data measured with the 4 m antenna and vertical coil alignment. A) Data measured during the pre-sampling survey in January 2018. B) Data measured during the post-sampling survey in January 2019 along the high resolution 3D ERT array.

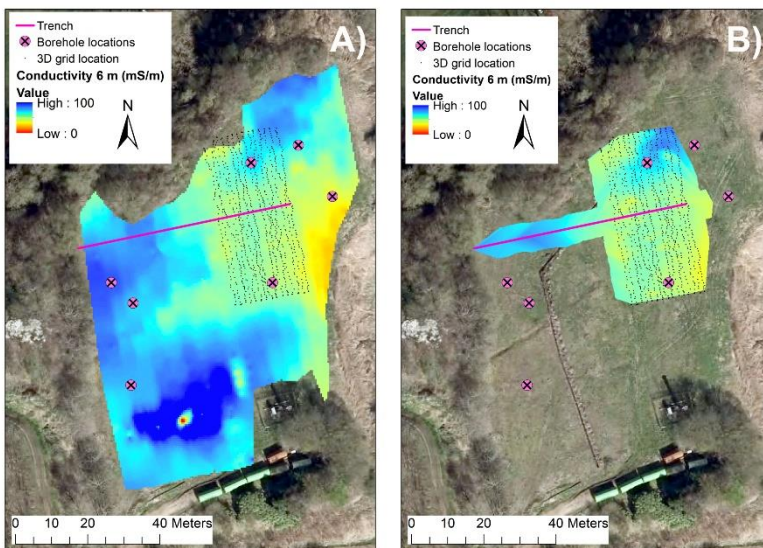


Figure 7: Electrical conductivity map at an investigation depth of 6 m below ground. This map was derived from the quadrature-phase data measured with the 4 m antenna and horizontal coil alignment. A) Data measured during the pre-sampling survey in January 2018. B) Data measured during the post-sampling survey in January 2019 along the high resolution 3D ERT array.

GPR

The ground penetrating radar data was processed with the software ReflexW from K. Sandmeier.

Fig. 10 summarizes the results of the GPR data with A to C displaying maps of the summed amplitude over 5 ns time windows at different depth ranges. Fig. D and C display two example radargrams corresponding to the profiles indicated by black dashed lines on the amplitude maps.

Interfaces of significant changes in electrical permittivity cause a strong reflection of the radar wave. Furthermore, depending on the conductivity and the heterogeneity of a layer, radar waves might be attenuated or diffracted in different ways. Therefore, summing up the signal amplitudes over a certain time window should provide an indication about changes in material properties within the respective time window.

Map A, corresponding to a depth of up to 0.25 m below surface, shows a pattern of very distinct linear features. They might correspond to different drainage patterns or tracks across the surface. Maps B and C, which correspond to depths between 0.25 and 0.75 m, indicate in the western part of the landfill a pattern, which is similar to the one seen on the conductivity maps of the EM data (see Fig. 7 to 9). This pattern showing a distinct change from North to South might be related to a different composition of the cover layer and/or a change in cover layer thickness. This change is also reflected in the radargrams D and C, which show a strong reflector at about 0.5 m and at 1 m depth in the southern half of the profile. These reflectors might correspond to an intermediate layer within the cover layer and to the interface between the cover layer and the waste. The invisibility of these reflectors in the northern half might indicate the absence of the intermediate layering. However, it is also possible that an overall higher conductivity of the cover layer material leads to a strong signal attenuation, which prohibits the detection of any interfaces.

On the eastern part of the landfill, no clear patterns are visible. Similarly, the radargrams indicate a strong attenuation of the signal (not shown here). This might be connected to a higher conductivity or a thinner cover layer on the eastern part of the landfill.

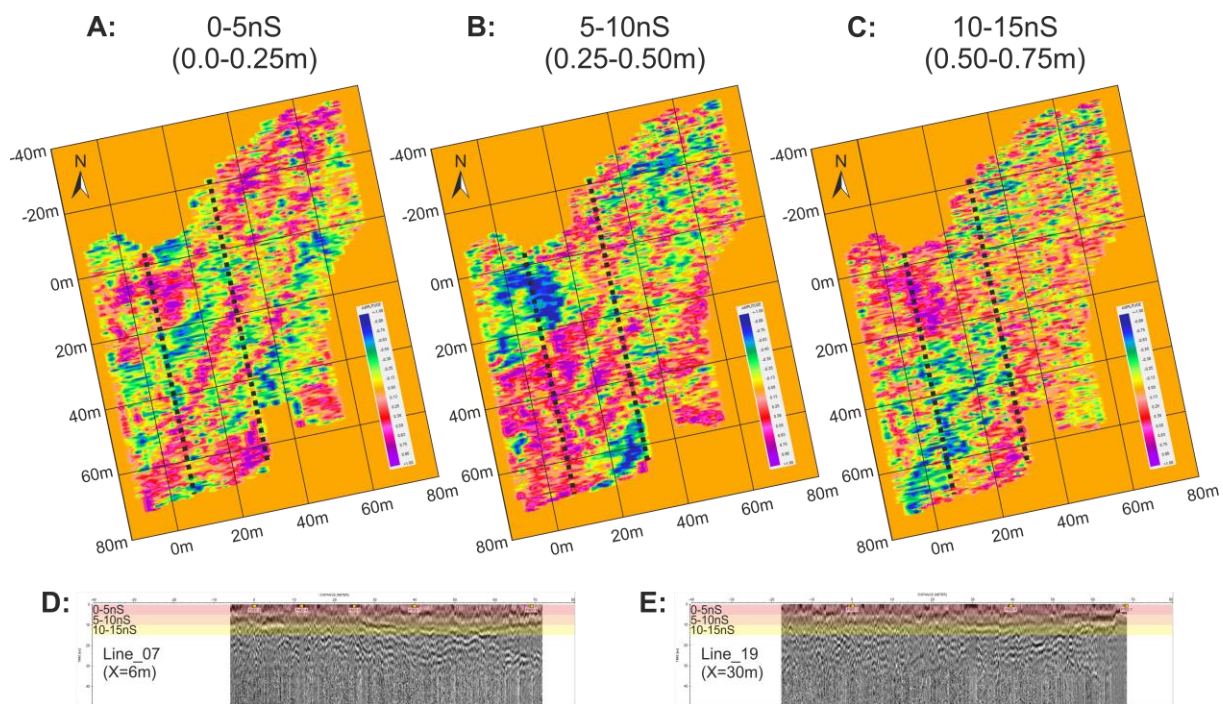


Figure 10: Results of the GPR measurement. A to C show maps of summed amplitudes over a 0.5 nS time window at different depths. D and E are example radargrams along the black dashed lines shown on the amplitude maps.

3D ERT

Data collected were first filtered by removing all measurements characterized by a repetition error larger than 5%. Then in order to weight the data in the inversion process, a data error model was built using the reciprocal data collected during the data acquisition. For the error model construction (see Fig. 11), the widely used approach proposed by Slater et al. (2000) was selected. Then weighted data were inverted with BERT (Günther et al., 2006; Rücker et al., 2006) using a robust constraint on the data and a smoothness constraint on the model. Model obtained with BERT (see Fig. 12) satisfied the error weighted chi-square, $\chi^2 = 1$ meaning that the data were fitted to their error level.

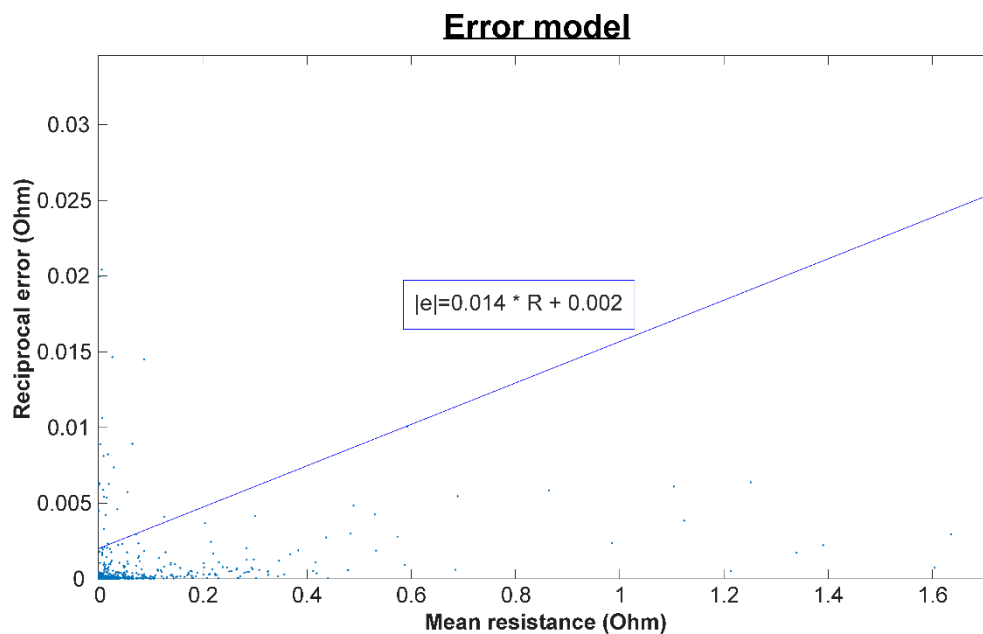


Figure 11: Data error model built using reciprocal measurements following the approach proposed in Slater et al. (2000).

At the surface of the 3D ERT model (see Fig. 12), higher electrical resistivity is observed. It may be attributed to unsaturated or frozen soil (given the climatic conditions encountered during data acquisition). The rippling pattern at the soil surface is a typical inversion artefact.

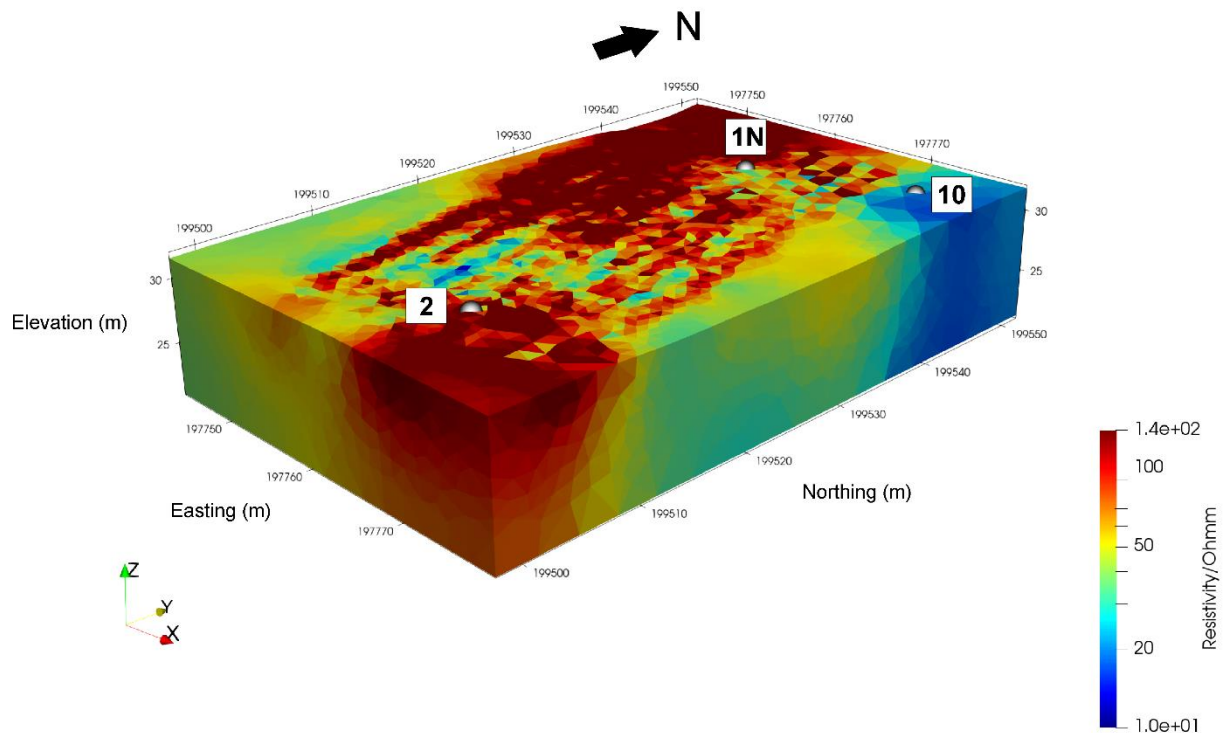


Figure 12: 3D electrical resistivity model

In order to analyse the results more at depth, one can show three transects passing by boreholes 2 and 1N (see Fig. 13). The image reveals a superficial layer with higher electrical resistivity (around 100 Ohm.m) that extends to a depth of 1 to 2 m. It corresponds to the unsaturated/frozen zone and seems to correlate well with the cover layer (see borehole logs). Underneath it, we observe a more conductive zone that may reveal a perched water/leachate table whose base is a less conductive (less saturated and possibly less pervious) layer, which tends to dip southward. In the northern part of the transects, very high conductive zone is observed at shallow depth which indicates more than likely a higher water/leachate content. That zone also tends to plunge southward below the intermediate more resistive zone.

2D ERT and IP

The high resolution ERT and IP profile that was collected along the direction of the trench just before it was dug is presented in Fig. 14. The resistivity model (Fig.14a) still displays the zonation observed in the 3D ERT model, i.e. from top to bottom:

- a high resistivity layer at the soil surface corresponding to the unsaturated sand of the cover layer;
- a more conductive layer probably related to a higher water content (saturated sand of the cover layer);
- a more resistive area likely related to unsaturated waste (the saturation contrast can be explained by the presence of plastic sheets or other types of waste that can act as a less permeable layer preventing water from reaching lower levels);
- a very conductive zone with high leachate content.

Chargeability model (Fig.14b) shows mainly two zones with contrasted electrical properties. The shallowest one is characterized by very low chargeabilities and corresponds to the cover layer mixed

with some waste. Below that layer, much higher chargeabilities are observed and seem to delineate the main waste body. The normalized chargeability model (Fig. 14c) offers maybe the best way to discriminate the cover layer from the main waste body. Unfortunately, the sensitivity at depth is not sufficient to detect the base of the landfill.

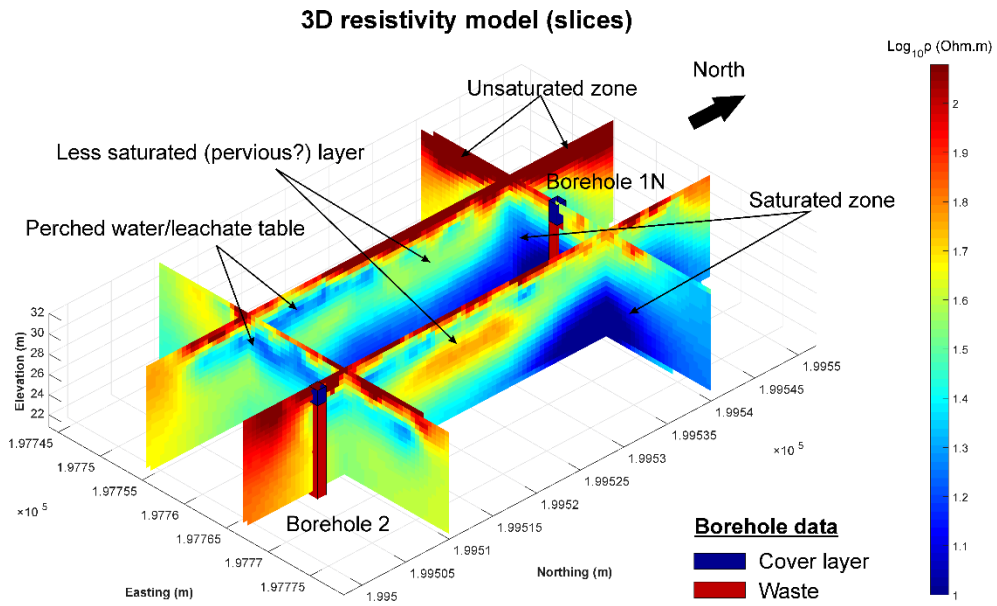


Figure 13: ERT transect passing by boreholes 2 and 1N

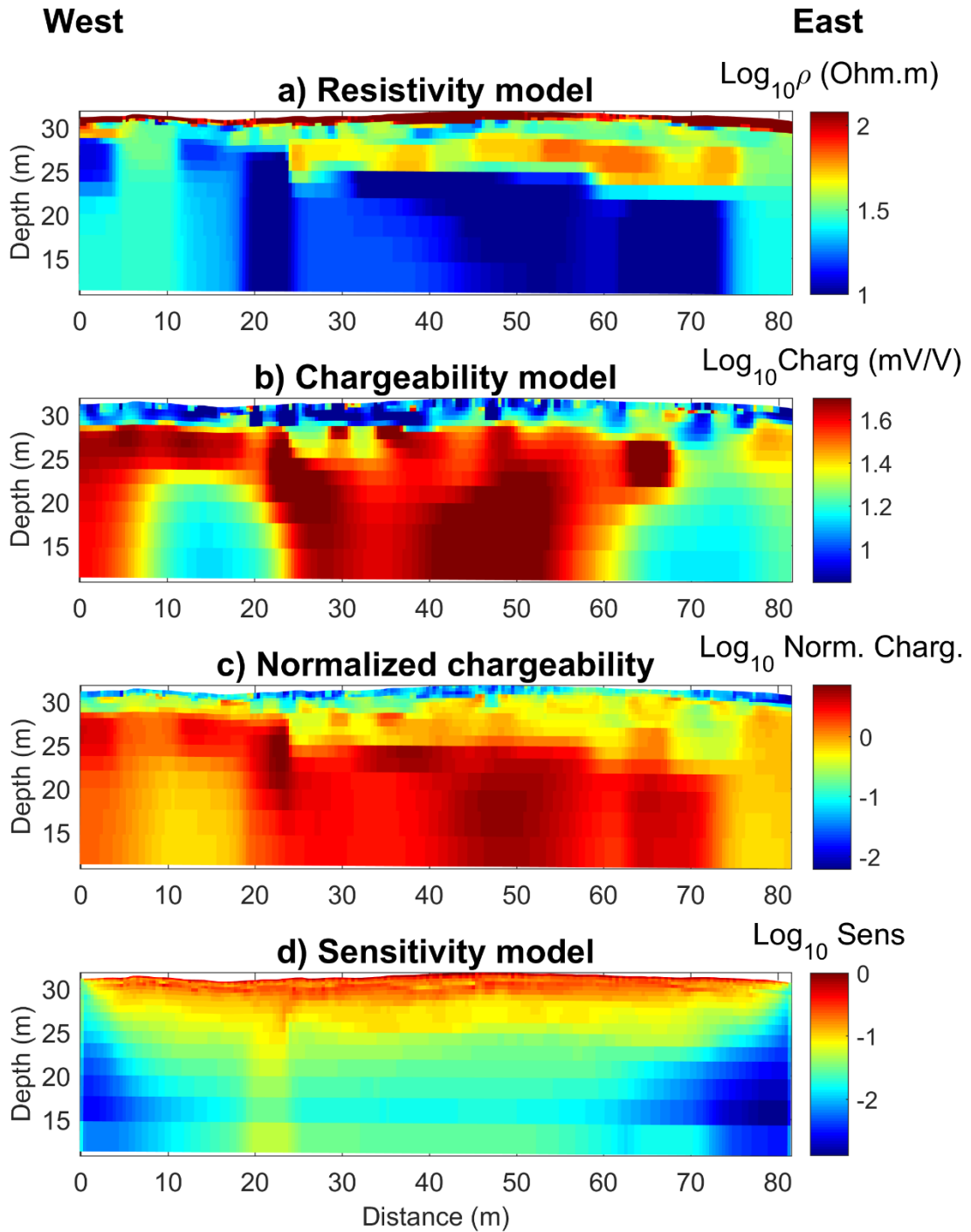


Figure 14: high resolution 2D ERT IP model with a) resistivity, b) chargeability, c) the normalized chargeability and d) sensitivity models.

Conclusions

The second geophysical survey in Meerhout allowed to refine our understanding of the lower part of the landfill where most of the drillings were conducted. EM maps globally show a good reproducibility from one survey to another. 3D ERT allowed to verify the continuity of several layers that were detected during the first survey. The high resolution ERT and IP profile that was acquired along the direction of the trench allowed to clearly detect the different zones in the landfill, especially by computing the normalized chargeability. Data collected also represent a good opportunity to calibrate and validate geophysical results with ground-truth data collected during trenching (see deliverable I1.3.4).

References

Dahlin, T., & Zhou, B. (2004). A numerical comparison of 2D resistivity imaging with 10 electrode arrays. *Geophysical Prospecting*, 52, 379-398.

Günther, T., Rücker, C., & Spitzer, K. (2006). Three-dimensional modelling and inversion of DC resistivity data incorporating topography—II. Inversion. *Geophysical Journal International*, 166(2), 506-517.

Rücker, C., Günther, T., & Spitzer, K. (2006). 3-d modeling and inversion of DC resistivity data incorporating topography—Part I: Modeling. *Geophys. J. Int.*, 166(2), 495-505.

Van Hoorde, M., Hermans, T., Dumont, G., & Nguyen, F. (2017). 3D electrical resistivity tomography of karstified formations using cross-line measurements. *Engineering geology*, 220, 123-132.

Contact

Feel free to contact us.

Local contact details:

BELGIUM	ATRASOL Cleantech Flanders / VITO OVAM SPAQuE Université de Liège	renaud.derijdt@atrasol.eu annick.vastiau@cleantechflanders.com ewille@ovam.be c.neculau@spaque.be f.nguyen@ulg.ac.be
FRANCE	SAS Les Champs Jouault	champsjouault@gmail.com
GERMANY	BAV	wolf@bavmail.de
THE UK	NERC	jecha@bgs.ac.uk

Coordination office:

BELGIUM	SPAQuE Boulevard d'Avroy 38 4000 Liège	c.neculau@spaque.be
----------------	--	---------------------
